Quantum Nondemolition Measurements with Optical Parametric Amplifiers for Ultrafast Universal Quantum Information Processing

Ryotatsu Yanagimoto,[1,*,‡] Rajveer Nehra,[2,†,‡] Ryan Hamerly,[3,4] Edwin Ng,[1,4] Alireza Marandi,[2] and Hideo Mabuchi[1]

[1] *E.L. Ginzton Laboratory, Stanford University, Stanford, California 94305, USA*
[2] *Department of Electrical Engineering, California Institute of Technology, Pasadena, California 91125, USA*
[3] *Research Laboratory of Electronics, MIT, 50 Vassar Street, Cambridge, Massachusetts 02139, USA*
[4] *Physics & Informatics Laboratories, NTT Research, Inc., Sunnyvale, California 94085, USA*

(Received 18 October 2022; accepted 8 March 2023; published 29 March 2023)

Realization of a room-temperature ultrafast photon-number-resolving quantum nondemolition (QND) measurement would have significant implications for photonic quantum information processing, enabling, for example, deterministic quantum computation in discrete-variable architectures, but the requirement for strong coupling has hampered the development of scalable implementations. In this work, we propose and analyze a nonlinear-optical route to photon-number-resolving QND using quadratic (i.e., $\chi^{(2)}$) nonlinear interactions. We show that the coherent pump field driving a frequency-detuned optical parametric amplifier (OPA) experiences displacements conditioned on the number of signal Bogoliubov excitations. A measurement of the pump displacement thus provides a QND measurement of the signal Bogoliubov excitations, projecting the signal mode to a squeezed photon-number state. We then show how our nonlinear OPA dynamics can be utilized to *deterministically* generate Gottesman-Kitaev-Preskill states with only additional Gaussian resources, offering an all-optical route for fault-tolerant quantum information processing in continuous-variable systems. Finally, we place these QND schemes into a more traditional context by highlighting analogies between the frequency-detuned optical parametric oscillator and multilevel atom-cavity quantum electrodynamics systems by showing how continuous monitoring of the outcoupled pump quadrature induces conditional localization of the intracavity signal mode onto squeezed photon-number states. Our analysis suggests that our proposal may be viable in near-term $\chi^{(2)}$ nonlinear nanophotonics, highlighting the rich potential of the OPA as a universal tool for ultrafast non-Gaussian quantum state engineering and quantum computation.

DOI: 10.1103/PRXQuantum.4.010333

I. INTRODUCTION

Quantum information science and engineering offer great potential for revolutionizing many fields, such as computation [1], communication [2], and metrology [3]. Among various physical systems that have been experimented with to encode and process quantum information, photonics offers significant advantages in room-temperature scalability and ultrafast operations [4]. Optical photons can span terahertz bandwidths and propagate over long distances with little decoherence, making them an ideal carrier of quantum information. In photonic quantum computation, information can be encoded and processed in both discrete-variable (DV) [5,6] and continuous-variable (CV) [7,8] architectures. However, the lack of strong optical nonlinearity has hindered the realization of deterministic two-qubit entangling gates in DV architectures [9–11] and non-Gaussian resources such as Gottesman-Kitaev-Preskill (GKP) states [12–15] in CV architectures; both of these are essential for building universal fault-tolerant quantum information processors. While some limitations of weak optical nonlinearity can be circumvented through measurement-based nonlinear operations using photon-number-resolving (PNR) measurement [16], the intrinsically probabilistic nature of these operations and the slow speed of conventional single-photon detectors (e.g., superconducting nanowires [17] and superconducting transition-edge sensors [18,19]) with complex cryogenic systems

*ryotatsu@stanford.edu
†rnehra@caltech.edu
‡These authors contributed equally to this work.

severely limit the scalability and computation clock rates in these architectures [9–11].

In this context, a realization of ultrafast, room-temperature PNR quantum nondemolition (QND) measurement [20–23] has significant implications in both DV and CV systems. In a PNR QND measurement, information about the number of photons is encoded in an auxiliary probe, and backaction is limited to (partial) projection onto a corresponding photon-number eigenstate [24,25]. Such an ultrafast QND measurement can not only replace the use of conventional superconducting PNR detectors but can also directly realize a deterministic two-qubit entangling gate, which enables deterministic DV optical quantum computation [26–28]. Additionally, the QND nature of the measurement offers unique opportunities for quantum engineering [29–31], communication [32], and metrology [33,34]. To realize a PNR QND measurement, it is typically necessary to engineer a resolvable single-photon energy shift, effectively leading to a strong coupling requirement $g/\kappa > 1$ (with coherent coupling rate g and decoherence rate κ). Since the pioneering work in atom-cavity quantum electrodynamics (QED) [35–39], strong coupling has been demonstrated in various physical systems [40–42]. However, concomitant implementations of the QND measurement in a scalable, high-bandwidth, and room-temperature platform have yet to be achieved.

In this work, we propose and analyze a nonlinear-optical route to PNR QND measurements and all-optical quantum state engineering for GKP states using a quadratic optical parametric amplifier (OPA). Compared with existing PNR QND measurement proposals [20–23] and GKP-state generation schemes [43,44] using cubic nonlinearities, our proposal with an OPA uses much stronger quadratic nonlinearity [45], offering a more experimentally viable route. Recently, $g/\kappa \sim 0.01$ was demonstrated with a quadratic nonlinear nanophotonic resonator [46,47], and even $g/\kappa \sim 10$ may be envisioned with ultrafast pulses [48].

In the following, we first show that the pump field of a frequency-detuned OPA experiences conditional displacements depending on the number of signal Bogoliubov excitations $\hat{N}_a$, while $\hat{N}_a$ is approximately preserved under the OPA dynamics. As a result, measuring the pump displacement allows one to perform a PNR QND measurement of $\hat{N}_a$. Next, we show that the nonlinear OPA dynamics can be utilized to perform a modular quadrature QND measurement [49,50] of the *pump* mode, with which we show a *near-deterministic* generation of the GKP states in the pump mode with only additional Gaussian resources, showing a nonlinear-optical route to universal fault-tolerant CV quantum information processing [15]. Finally, we bridge the physics of these QND schemes to a more traditional context by establishing analogies between a frequency-detuned optical parametric oscillator (OPO) and multilevel atom-cavity QED systems. We observe conditional localization of the intracavity state to the squeezed Fock state ladder, which in experiments can be inferred from the pump homodyne record without monitoring the signal photon loss at all, using a quantum filter [51].

II. PNR QND MEASUREMENTS WITH A FREQUENCY-DETUNED OPA

We consider a frequency-detuned single-mode quadratic (i.e., $\chi^{(2)}$) nonlinear Hamiltonian

$$\hat{H} = g(\hat{a}^{\dagger 2}\hat{b} + \hat{a}^2\hat{b}^\dagger) + \delta\hat{a}^\dagger\hat{a}, \tag{1}$$

where $\hat{a}$ and $\hat{b}$ represent annihilation operators for the signal (i.e., fundamental harmonic) and the pump (i.e., second harmonic) modes, respectively, and $g > 0$ is the nonlinear coupling strength. We assume a non-negative frequency detuning between the signal and the pump $\delta \geq 0$ without loss of generality. It is worth noting that various photonic systems can be described by Eq. (1), including high-Q microring resonators [47], photonic crystal cavities [52,53], temporally trapped ultrashort pulses [48], and superconducting microwave circuits [54], and our results do not rely on a specific physical realization. For the derivation of the Hamiltonian, see Appendix A.

To treat the pump coherent amplitude (which may be large in many practical scenarios) in a parameterized way, we move to a displaced frame given by a unitary $\hat{D}_b(\beta) = \exp\left(\beta\hat{b}^\dagger - \beta^*\hat{b}\right)$, where the mean field of the pump mode is "factored out" as

$$|\psi(t)\rangle = \hat{D}_b(\beta)\,|\varphi(t)\rangle\,, \tag{2}$$

where $|\psi(t)\rangle$ and $|\varphi(t)\rangle$ are the system states in the laboratory frame and the displaced frame, respectively. We assume β is real and positive without loss of generality. Physically, $|\varphi(t)\rangle$ accounts for quantum fluctuations around the mean field, whose dynamics follow $i\partial_t\,|\varphi(t)\rangle = \hat{H}_D\,|\varphi(t)\rangle$, where the Hamiltonian

$$\hat{H}_D = \hat{D}_b^\dagger(\beta)\hat{H}\hat{D}_b(\beta) = \hat{H}_{\rm NL} + \hat{H}_Q \tag{3}$$

is composed of a cubic nonlinear term and a quadratic term

$$\hat{H}_{\rm NL} = g(\hat{a}^{\dagger 2}\hat{b} + \hat{a}^2\hat{b}^\dagger), \quad \hat{H}_Q = \delta\hat{a}^\dagger\hat{a} + \frac{r}{2}\left(\hat{a}^{\dagger 2} + \hat{a}^2\right), \tag{4}$$

with $r = 2g\beta$. From here on, we assume we are in the displaced frame unless specified otherwise.

An OPA is realized for an initial state $|\varphi(0)\rangle = |\varphi_a(0)\rangle\,|\varphi_b(0)\rangle$ with $|\varphi_b(0)\rangle = |0\rangle$, whose pump state is a coherent state with displacement β in the laboratory frame. A conventional approach to analyze an OPA is to use an undepleted pump approximation, where the pump state remains invariant throughout the dynamics. As shown in

Ref. [55], this approximation is equivalent to ignoring $\hat{H}_{\mathrm{NL}}$ in $\hat{H}_D$, leading to single-mode squeezing of the signal state, which is the expected behavior of an OPA in the regime of Gaussian quantum optics [56].

Under stronger nonlinearity where the undepleted pump approximation breaks down, the contribution of the nonlinear term $\hat{H}_{\mathrm{NL}}$ induces non-Gaussian quantum features, e.g., signal-pump entanglement [55,57,58], for which we critically lack a qualitative physical description. In the following, as a main result of this work, we show a concise description of the nonlinear quantum behavior of a frequency-detuned OPA as a QND measurement of signal photons in the squeezed photon number basis. Our analysis adopts the Hamiltonian transformation recently introduced in Ref. [59].

Assuming a relatively large frequency detuning $\delta > r$, we can rewrite $\hat{H}_Q$ as

$$\hat{H}_Q = \delta \hat{a}^\dagger \hat{a} + \frac{r}{2}\left(\hat{a}^{\dagger 2} + \hat{a}^2\right) = \Delta \hat{A}^\dagger \hat{A} + \text{const}, \tag{5}$$

where $\hat{A} = \hat{a}\cosh u + \hat{a}^\dagger \sinh u$ corresponds to the annihilation operator for Bogoliubov excitations, with $\Delta = \sqrt{\delta^2 - r^2}$ and $u = \tanh^{-1}(r/\delta)/2$. Intuitively, we can interpret $\hat{A}$ as an annihilation operator of a photon excitation in a squeezed photon number basis. The nonlinear Hamiltonian can then be rewritten in terms of the Bogoliubov operators as

$$\hat{H}_{\mathrm{NL}} = g\left\{\cosh^2 u\, \hat{A}^{\dagger 2} + \sinh^2 u\, \hat{A}^2 - \sinh 2u \left(\hat{A}^\dagger \hat{A} + \frac{1}{2}\right)\right\}\hat{b} + \text{H.c.} \tag{6}$$

For the rest of this work, we assume that the magnitude of $\hat{H}_Q$ dominates over $\hat{H}_{\mathrm{NL}}$, i.e., $ge^{2u} \ll \Delta$, which can always be achieved by appropriately choosing δ and r (i.e., β). Under these conditions, the contributions from the rapidly rotating terms containing $\hat{A}^2$ and $\hat{A}^{\dagger 2}$ average out, allowing us to perform a rotating-wave approximation [59–61]. We thus have

$$\hat{H}_D \approx -2\tilde{g}\left(\hat{N}_a + \frac{1}{2}\right)\hat{x}_b + \Delta \hat{N}_a + \text{const}, \tag{7}$$

where $\hat{N}_a = \hat{A}^\dagger \hat{A}$, $\hat{x}_b = (\hat{b} + \hat{b}^\dagger)/2$, and $\tilde{g} = g \sinh 2u$.

In the Heisenberg picture, we analytically solve the operator dynamics under Eq. (7) as

$$\hat{N}_a(t) \approx \hat{N}_a(0), \quad \hat{p}_b(t) \approx \tilde{g}t\left(\hat{N}_a(0) + \frac{1}{2}\right) + \hat{p}_b(0), \tag{8}$$

where $\hat{p}_b = (\hat{b} - \hat{b}^\dagger)/2i$ is the p-quadrature operator of the pump mode. From Eq. (8), we note that the pump mode $\hat{p}_b$ experiences a displacement conditioned on the value of $\hat{N}_a$, leading to a specific signal-pump entanglement structure. Additionally, $[\hat{H}_D, \hat{N}_a] \approx 0$ ensures that the value of $\hat{N}_a$ is not disturbed during the system evolution. As a result, homodyne measurement of $\hat{p}_b$ allows us to infer $\hat{N}_a$ *without* performing a destructive measurement on the signal mode, thereby realizing a QND measurement of $\hat{N}_a$. Depending on the measurement result for $\hat{p}_b$, the signal state is projected onto an eigenstate of $\hat{N}_a$ with eigenvalue N_a, i.e., a squeezed photon-number state $|N_a\rangle = 1/(\sqrt{N_a!})\hat{A}^{\dagger N_a}|0\rangle$. This situation is summarized in Fig. 1.

The performance of our PNR QND measurement depends on the measurement accuracy of $\hat{p}_b$, which is limited by the quadrature fluctuations of the probe pump state. Intuitively, the conditional displacement $d = \tilde{g}t$ needs to be sufficiently large compared with the width of the p-quadrature fluctuations $w = \sqrt{\langle\varphi_b|\hat{p}_b^2|\varphi_b\rangle - \langle\varphi_b|\hat{p}_b|\varphi_b\rangle^2}$ to infer the value of $\hat{N}_a$ with high confidence. In Fig. 1, we show the result of a full-quantum simulation of nonlinear OPA dynamics with an initial squeezed-vacuum pump state with $w = 1/4$. The final pump state exhibits multiple Gaussian peaks in the phase space separated by the distance d, each of which corresponds to a different number of signal Bogoliubov excitations $\hat{N}_a$. Because we have $d/w = 4$ ($d = 1, w = 1/4$) for the parameters used for Fig. 1, conditioning on the measurement result for $\hat{p}_b$ projects the signal state to a squeezed photon-number state with fidelity that can exceed 90% with the assumed system parameters.

To establish more quantitative connections between the performance of the measurement and the squeezing of the probe-pump quadrature fluctuations, we provide the expressions for the Kraus operators of our QND measurement protocol. From Eq. (7), the Kraus operators can be expressed as

$$\hat{M}(p_b) = \sum_{N_a=0}^{\infty} \mathcal{C}_{N_a}(p_b)\,|N_a\rangle\langle N_a|\,, \tag{9}$$

with $\mathcal{C}_{N_a}(p_b) = e^{-i\Delta N_a t}\langle p_b - d\,(N_a + 1/2)|\varphi_b\rangle$ being the complex probability amplitudes for the measurement outcomes, where $|p_b\rangle$ is an eigenstate of $\hat{p}_b$ with eigenvalue p_b (see Appendix B for the full derivations). The Kraus operators are related to a positive-operator-valued measure (POVM) with elements

$$\hat{F}(p_b) = \hat{M}^\dagger(p_b)\hat{M}(p_b) = \sum_{N_a=0}^{\infty} |\mathcal{C}_{N_a}(p_b)|^2\,|N_a\rangle\langle N_a|\,. \tag{10}$$

Physically, the outcome of a complete pump homodyne measurement p_b follows a probability distribution $P(p_b) = \langle\varphi_a|\hat{F}(p_b)|\varphi_a\rangle$, and conditioned on the outcome p_b, the postmeasurement signal state becomes $|\varphi_a'(p_b)\rangle = \hat{M}(p_b)\,|\varphi_a(0)\rangle$ up to normalization.

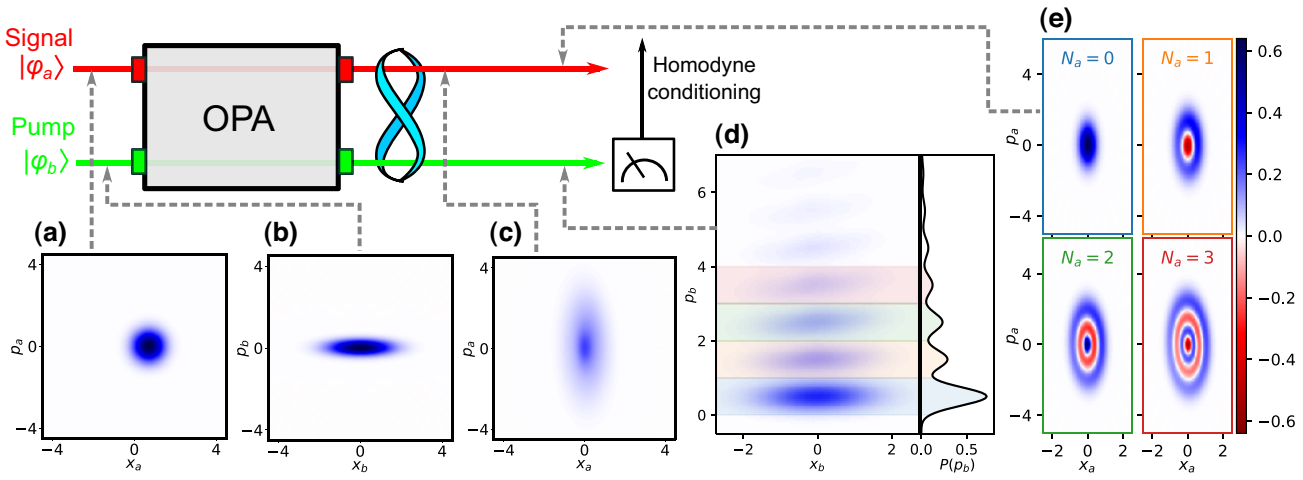

FIG. 1. Our PNR QND measurement scheme using nonlinear quantum behavior of an OPA, where the phase-space representation (i.e., Wigner functions) of the system state at each step of the protocol is shown using numerical data. For the numerical simulation, we consider an initial coherent signal state $|\varphi_a(0)\rangle = |\alpha = 0.7\rangle$ [shown in (a)], and we assume a p-squeezed vacuum state with width $w = 1/4$ as an initial pump state [shown in (b)]. The signal and pump states interact through a frequency-detuned OPA, whose dynamics induce conditional p displacements of the pump field depending on the number of signal Bogoliubov excitations $\hat{N}_a$. Concurrently, the OPA dynamics also cause conditional rotations on the signal Bogoliubov excitation depending on $\hat{x}_b$, leading to the phase spread of the final unconditional signal state [shown in (c)]. A complete p-homodyne measurement on the final pump state acts as a QND measurement of $\hat{N}_a$ and projects the signal mode on a squeezed photon-number state, which is an eigenstate of $\hat{N}_a$. (d) The final pump state shown with the p-quadrature distribution $P(p_b)$. (e) Ensemble-averaged signal states conditioned on the outcome of the homodyne measurement within an interval $\tilde{g}t(N_a - 1) \le \hat{p}_b \le \tilde{g}t(N_a + 1)$. We use the system parameters of $\Delta/g = 150$ and $\tilde{g}/g = 1$, and the total interaction time of $gt = 1$.

It is worth mentioning that the POVM (9) is not completely selective with respect to N_a, because $\hat{F}(p_b)$ is not solely composed of a single squeezed-Fock-state projector $|N_a\rangle\langle N_a|$. To characterize the mixedness of the POVM, it is insightful to consider its relative weights on the squeezed-Fock-state projectors

$$W_{N_a}(p_b) = \frac{|C_{N_a}(p_b)|^2}{\sum_{N_a'=0}^{\infty} |C_{N_a'}(p_b)|^2}, \tag{11}$$

which can be intuitively interpreted as the weights applied to $|N_a\rangle$ conditioned on the homodyne outcome (see Appendix B for full discussions). In particular, $W_{N_a}(p_b) = 1$ implies the postmeasurement state conditioned on the homodyne outcome p_b is a pure squeezed Fock state $|N_a\rangle$.

In Fig. 2(a), we show the purity of the POVM $\gamma(\hat{F}(p_b)) = \mathrm{tr}(\hat{F}^2(p_b))/\mathrm{tr}(\hat{F}(p_b))^2$ [62] as a function of the homodyne measurement outcome p_b, where we assume squeezed vacuum states with width w as the initial probe state. As can be seen from Fig. 2(a), using a probe state with smaller w increases the purity of the POVM for a given d, projecting the signal to a squeezed photon-number state with higher fidelity. From an experimental perspective, squeezing the pump quadrature allows us to implement a PNR QND measurement with a shorter nonlinear interaction time and hence potentially lower propagation loss. In Fig. 2(b), we show the relative weights of squeezed-Fock-state projectors $W_{N_a}(p_b)$, where we can see that the homodyne outcome of $p_b \approx d(N_a + 1/2)$ dominantly projects the input state to $|N_a\rangle$. Readers can also refer to Ref. [63] for general discussions on nonlinear amplifiers and quantum measurements that they can implement.

In contrast to the phase-insensitive photon-number tomography attainable by conventional PNR QND measurements [20–22], our scheme can perform PNR QND measurement in an arbitrary squeezed photon number basis, enabling phase-sensitive squeeze tomography [64, 65], from which we can obtain phase information about the state under tomographic reconstruction. Here, introducing a complex phase to the pump displacement β changes the rotation angle of the basis, while the ratio r/δ determines the squeezing factor. The measurement basis gets more squeezed for $r/\delta \to 1$, where we can have a larger enhancement factor of nonlinear coupling $\tilde{g}/g$. In the other limit of $r/\delta \to 0$, the measurement basis converges to the (nonsqueezed) photon-number state basis, which comes with a cost of vanishing effective nonlinear coupling $\tilde{g}/g \to 0$. It is worth mentioning that additional Gaussian operations can enable flexible control over the measurement basis without compromising the nonlinear coupling. For this purpose, we can apply a pair of opposite squeezing operations $\hat{S}_a$ and $\hat{S}_a^\dagger$ to the signal state before and after evolving under $\hat{H}_D$, respectively, which transforms the

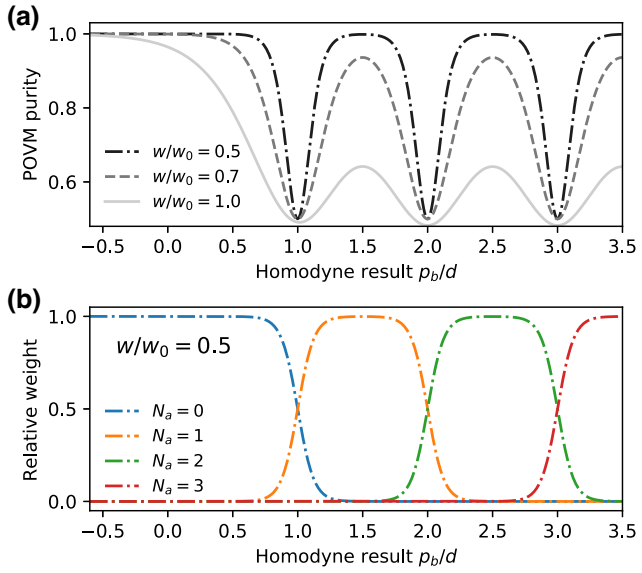

FIG. 2. (a) Purity of the POVM for our QND measurement protocol [62] as a function of the pump homodyne outcome p_b. We consider a Gaussian probe pump state $|\varphi_b(0)\rangle$ with various widths w, where w below the vacuum level $w_0 = 1/2$ indicates that $|\varphi_b(0)\rangle$ is a squeezed vacuum. (b) Relative weights of squeezed-Fock-state projector $W_{N_a}(p_b)$ in the POVM as a function of p_b for $w/w_0 = 0.5$. We assume conditional displacement of $d = \tilde{g}t = 1.0$ for all plots.

measurement basis so that $\hat{N}_{\rm eff} = \hat{A}^\dagger_{\rm eff}\hat{A}_{\rm eff}$ is measured with $\hat{A}_{\rm eff} = \hat{S}_a^\dagger \hat{A} \hat{S}_a$ [66]. By choosing $\hat{S}_a$ such that $\hat{A}_{\rm eff} = \hat{a}$, we realize a QND measurement of the normal photon number $\hat{n}_a = \hat{a}^\dagger\hat{a}$ without resorting to the limit of $r/\delta \to 0$. Such a pair of squeezing and antisqueezing operations was experimentally demonstrated on pulsed nonlinear nanophotonics as reported in Ref. [67]. Full analysis of the effects of loss of the external squeezing operations is provided in Appendix E.

III. QUANTUM STATE ENGINEERING FOR GOTTESMAN-KITAEV-PRESKILL STATES

While our focus so far has been on QND measurement of the signal excitations, we now show that one can also perform a QND measurement of the pump field quadratures using the same physics of the nonlinear OPA dynamics. For this, we use the operator dynamics under Eq. (7) as

$$\hat{x}_b(t) = \hat{x}_b(0), \quad \hat{A}(t) = e^{i(2\tilde{g}t\hat{x}_b(0) - \Delta t)}\hat{A}(0), \tag{12}$$

where the information about $2\tilde{g}t\hat{x}_b - \Delta t$ is encoded in the phase of $\hat{A}$ up to the modulus of 2π. Therefore, the measured phase of $\hat{A}$, e.g., with a general-dyne measurement [68–70], indirectly infers the value of $\hat{x}_b$ modulo $\mu = \pi/\tilde{g}t$, which projects the pump mode to $\hat{x}_b = x_\phi \pmod{\mu}$ for a phase measurement outcome of ϕ, where we denote $x_\phi = (\phi + \Delta t)/2\tilde{g}t \pmod{\mu}$. The pump quadrature $\hat{x}_b$ itself remains constant throughout the dynamics due to $[\hat{x}_b, \hat{H}_D] \approx 0$, which ensures the QND nature of the measurement. Such modular quadrature measurements play central roles in contemporary CV quantum information processing, e.g., for deterministic generation, stabilization, and quantum error correction with GKP states [14,49,50]. In the following, we demonstrate a preparation of an approximate GKP state using the nonlinear dynamics of an OPA, where only additional Gaussian resources (i.e., Gaussian initial states, measurements, and feedforward operations) are used. Our proposal for generating GKP states adapts the protocols introduced in Refs. [14,49], with crucial technical differences stemming from the nonlinear dynamics of frequency-detuned OPAs.

For the following discussions, we denote a coherent excitation of the Bogoliubov signal mode as $|A\rangle$. Physically, $|A\rangle$ is a displaced squeezed state and is an eigenstate of the operator $\hat{A}$ with eigenvalue A. As shown in Fig. 3, we prepare the initial signal state $|A_0\rangle$ with $A_0 > 0$ as a "meter" state for the phase shift. For the initial pump state, we assume a p-squeezed vacuum with width $w/4$ along the p quadrature.

After propagation through a nonlinear OPA for time t, we perform a phase measurement on $\hat{A}$ by a complete general-dyne measurement [68], which projects the signal mode on the measurement basis of displaced squeezed states $\{|e^{i\phi}(A_0 + \epsilon)\rangle\}$. Here, the measurement basis is parameterized by the radius $(A_0 + \epsilon) \geq 0$ and the phase ϕ (see Appendix F for full details on the construction of a general-dyne measurement). The performance of the phase measurement can be further improved by adaptive measurement schemes [69,70]. For the preparation of a GKP state, a modular quadrature measurement with modulus $\mu = \sqrt{2\pi}$ is desired, which sets the interaction time $\tilde{g}t = \sqrt{\pi/2}$.

When the magnitude of the meter state A_0 is much larger than the vacuum noise level, the measurement outcome is expected to be exponentially localized around $|\epsilon| \ll A_0$. Assuming this condition is met, the postmeasurement pump state becomes

$$|\varphi_b'\rangle \approx \hat{D}_b(x_\phi)\hat{D}_b\left(i\sqrt{\pi/2}\,\lfloor A_0 \rfloor^2\right)\left|\tilde{0}\right\rangle, \tag{13}$$

which can be transformed to an approximate GKP logical state

$$\left|\tilde{0}\right\rangle \propto \sum_{n=-\infty}^{\infty} e^{-\frac{w^2(n\sqrt{2\pi}+x_\phi)^2}{4}}\hat{D}_b(n\sqrt{2\pi})\,|\kappa\rangle \tag{14}$$

via trivial displacement operations (see Appendix C for more details). Here, $\lfloor\cdot\rfloor$ is a floor function, and $|\kappa\rangle$ is an x-squeezed vacuum with width $\kappa = \sqrt{\langle\hat{x}_b^2\rangle - \langle\hat{x}_b\rangle^2} =$

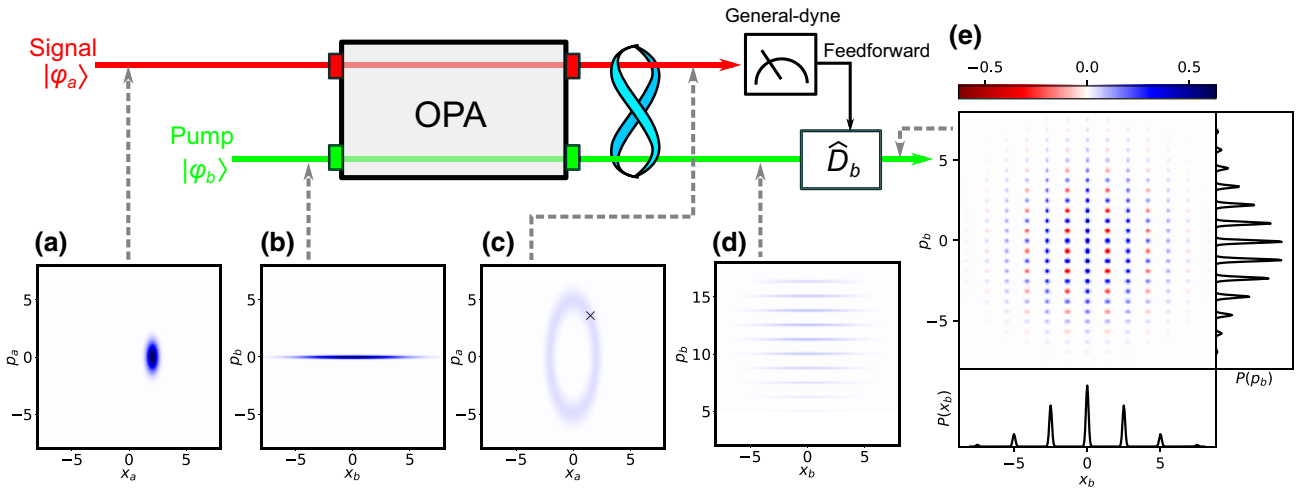

FIG. 3. Generation of a symmetric GKP state with 15 dB of squeezing using nonlinear quantum dynamics of an OPA. The initial signal state is $|A_0\rangle$ [shown in (a)], and the pump state, which is instantiated as a 15-dB p-squeezed vacuum [shown in (b)], interact through a frequency-detuned quadratic OPA Hamiltonian. A complete general-dyne measurement is performed on the final signal mode [shown in (c)] to measure the phase of the signal Bogoliubov excitation ϕ. Conditioned on the phase measurement outcome, the final pump state [shown in (d)] collapses to an approximate GKP state up to extra displacements, which can be compensated by feedforward operations. The Wigner function and the marginal quadrature distributions of the resultant approximate GKP state are shown in (e). We assume a signal measurement outcome of $\epsilon = 0.1$ and $\phi = \pi/4$, whose centroid is indicated by a black cross in (c). For the simulations, we use the Hamiltonian (7) with $\tilde{g}/g = 1.0$ and $\Delta = 100$.

$1/2\sqrt{\pi}A_0$ along the x quadrature. It is worth mentioning that this GKP generation scheme is nearly deterministic, because an extra displacement $\hat{D}_b(\hat{x}_\phi)$ induced by the probabilistic phase readout ϕ can be largely compensated by the trivial feedforward displacement operations. The resultant GKP state becomes symmetric when $w = \kappa$ holds true, corresponding to $A_0 = 1/2\sqrt{\pi}w$.

In Fig. 3, we show the results of our numerical simulations showing the generation of a symmetric GKP state with a squeezing level of 15 dB (beyond the error correction threshold of approximately 10 dB [71,72]). Compared with existing nonlinear-optical GKP state generation schemes using cross-phase modulation [43,44], our approach uses much stronger quadratic nonlinearities, which may offer more viable prospects for non-Gaussian state engineering at room temperature.

It is important to note that, in addition to the GKP logical states, we need nontrivial superpositions of them, e.g., GKP magic states [15,73,74], to realize universal quantum computation. Since our scheme cannot directly generate GKP magic states from Gaussian resources, this important challenge of realizing a universal gate set for GKP codes has to be addressed separately. To this end, Baragiola *et al.* [15] showed that generation of GKP magic states is possible with only additional Gaussian resources, provided we have access to a supply of GKP logical states, for which our scheme can serve as an efficient source. This means that a nonlinear OPA is, in principle, a sufficient resource to realize universal nonlinear-optical quantum computation with additional all-Gaussian resources.

IV. NONLINEAR QUANTUM FLUCTUATIONS IN OPO DYNAMICS

An important application of parametric interactions is an OPO, which is realized by pumping a quadratic nonlinear resonator with an external drive field. In the absence of signal loss, a resonant OPO with zero frequency detuning $\delta = 0$ has two transient states, i.e., odd and even signal cat states comprising the quantum superposition of π-phase-shifted coherent states. The presence of a finite signal loss leads to spontaneous switching of the parity of the cat states, devolving the cat states into incoherent mixtures of the original coherent states [75,76], which is reminiscent of the spontaneous quantum jumps observed in a two-level atom-cavity QED system [77]. Here, we show that a frequency-detuned OPO exhibits behavior reminiscent of *multilevel* atom-cavity QED, where the signal photon loss induces quantum jumps among the signal states in the squeezed Fock state ladder.

We introduce an external pump drive for an OPO given by the Hamiltonian term $\hat{H}_{\rm drive} = i\lambda(\hat{b}^\dagger - \hat{b})$, and the outcoupling pump loss is characterized by the Lindblad operator $\hat{L}_b = \sqrt{\kappa_b}(\hat{b} + \beta)$ (in the laboratory frame $\hat{L}_b = \sqrt{\kappa_b}\hat{b}$). In the absence of signal loss, the pump operator dynamics follow

$$i\partial_t\hat{b} = -\tilde{g}\left(\hat{N}_a + \frac{1}{2}\right) - \frac{i\kappa_b}{2}(\hat{b} + \beta) + i\lambda, \tag{15}$$

while $\hat{N}_a$ remains constant. For a choice of $\lambda = \kappa_b\beta/2$, we have stationary states $|N_a\rangle\left|\beta_{N_a}\right\rangle$ for $N_a \in \mathbb{Z}^+$, where

$|\beta_{N_a}\rangle$ is a coherent pump state with displacement $\beta_{N_a} = 2i\kappa_b^{-1}\tilde{g}(N_a + 1/2)$. Since β_{N_a} depends on N_a, the pump photons leaving the OPO carry out information about N_a, which plays the role of a weak continuous QND measurement of $\hat{N}_a$. Thus, by our monitoring the outcoupled pump field, the system (pump-signal) state is expected to conditionally collapse to one of the stationary states $|N_a\rangle\,|\beta_{N_a}\rangle$.

Let us now consider the effects of a finite signal loss. When a signal photon is lost from $|\beta_{N_a}\rangle$, the intracavity signal state experiences a quantum jump as $|N_a\rangle \mapsto \hat{a}\,|N_a\rangle$, resulting in the signal mode given as

$$\cosh u\,\sqrt{N_a}\,|N_a - 1\rangle - \sinh u\,\sqrt{N_a + 1}\,|N_a + 1\rangle\,. \quad (16)$$

This implies that a loss of a signal photon, corresponding to a photon subtraction from a squeezed photon-number state, induces a discrete jump of the Bogoliubov excitation $N_a \mapsto N_a \pm 1$, both in the positive direction and in the negative direction. Note that the flow is biased toward the negative direction because $\cosh u > \sinh u$.

Because of the quantum correlations between $\hat{N}_a$ and $\hat{p}_b$, the occurrence of such a quantum jump can be inferred from the record on the pump homodyne measurement without the signal loss photons being monitored at all. To emulate this situation, we perform numerical simulations of a stochastic master equation [51] unraveled by a pump p-homodyne measurement, while we do not monitor signal loss photons. As shown in Fig. 4(a), we observe correlated spontaneous jumps in $\langle\hat{N}_a\rangle$ and $\langle\hat{p}_b\rangle$ showing multilevel plateaus corresponding to the production of squeezed photon-number states, which can be inferred solely from the pump homodyne record [77,78]. Such discrete behaviors emerging from a continuous-variable system under the monitoring of only continuous observables are illuminating manifestations of the intrinsic quantum nature of photons. When the system is found in $|N_a = 0\rangle\,|\beta_{N_a=0}\rangle$, the signal state is in a squeezed vacuum, whose squeezing level can conditionally exceed the -3-dB limit of an OPO intracavity steady-state squeezing [79] [see Fig. 4(b)]. Note that this phenomenon exhibiting strong *signal* squeezing is distinct from the physics unraveled in Ref. [59], where more than 3 dB of squeezing is realized in the *pump* mode of an OPO.

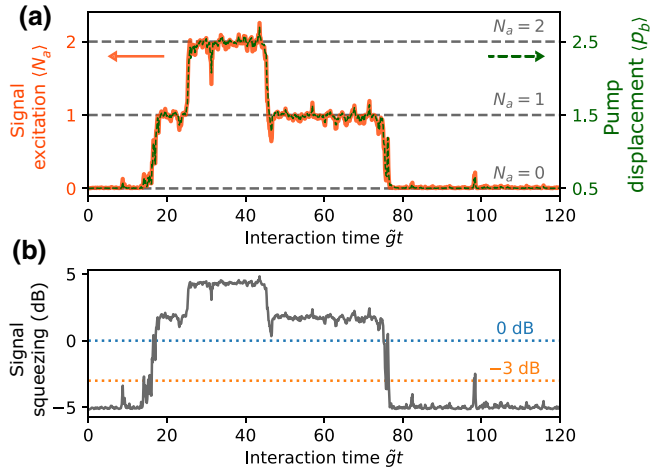

FIG. 4. A typical stochastic master equation quantum trajectory of the OPO dynamics unraveled by a continuous pump p-homodyne measurement. (a) Trajectories of $\langle\hat{N}_a\rangle$ (solid orange line, left axis) and $\langle\hat{p}_b\rangle$ (dashed green line, right axis) compared with the expected levels of the plateaus $\langle\hat{p}_b\rangle = \mathrm{Im}(\beta_{N_a})$ (dashed gray lines). (b) A trajectory of the signal x-quadrature squeezing compared with the quadrature noise levels for a vacuum (0 dB, dotted blue line) and the squeezing limit for an OPO steady-state (-3 dB, dotted orange line). We use Eq. (7) with system parameters $\Delta/g = 100$, $\tilde{g}/g = 1.5$, $\kappa_a/g = 0.03$, and $\kappa_b/g = 3.0$.

V. EXPERIMENTAL PROSPECTS

We discuss experimental requirements for the implementation of our PNR QND measurement scheme in the single-photon regime. For this purpose, we assume large squeezing factors for all the fields involved in the dynamics, i.e., signal Bogoliubov excitation and probe pump state, to study the potential of squeezing to enhance effective nonlinear coupling. Assuming a similar level of loss and similar squeezing factors for the signal and the pump, i.e., $\kappa_a \sim \kappa_b$ and $w \sim e^{-u} \ll 1$, an experimental requirement for our scheme becomes

$$\frac{g}{\kappa_a} \gtrsim w \quad (17)$$

(see Appendix D for full discussions), where the squiggly symbol denotes approximate equality (inequality) faithful up to factors of order of unity. Notice that compared with the normal definition of strong coupling $g/\kappa_a > 1$, the requirement (17) is reduced by the squeezing of the probe pump mode. For instance, applying 15 dB of squeezing on the initial pump can approximately reduce the requirement for g/κ_a by a factor of $w^{-1} \sim 5.6$. A promising nonlinear-optical realization of Eq. (1) is by means of a high-Q microring resonator, where $g/\kappa_a \sim 0.01$ was recently realized in indium gallium phosphide nanophotonics [46] and thin-film lithium niobate nanophotonics [47]. Moreover, ultrafast pulse operations enabled by advanced dispersion engineering can further enhance the nonlinear coupling by simultaneously leveraging both temporal and spatial field confinements, with which $g/\kappa_a \sim 10$ may be possible [48]. When realized in a single-path manner, such an implementation with ultrashort pulses may enable PNR QND measurements with terahertz through rates. These numbers suggest bright prospects for the potential realization of our proposed scheme in near-term $\chi^{(2)}$ nonlinear nanophotonics.

VI. CONCLUSION

In this work, we propose and analyze a scheme for PNR QND measurement and quantum state engineering using the nonlinear quantum behavior of an OPA. We first show that the pump mode driving a frequency-detuned OPA experiences conditional displacements depending on the number of signal Bogoliubov excitations $\hat{N}_a$, enabling one to measure $\hat{N}_a$ nondestructively via a pump homodyne detection. Such PNR QND measurements allow high-efficiency ultrafast PNR measurements (replacing the use of conventional slow superconducting detectors) and a deterministic implementation of a photon-photon entangling gate [26,27], providing all the necessary elements for deterministic room-temperature DV photonic quantum computation at ultrafast clock rates.

We then show that the nonlinear OPA dynamics can be utilized to realize a modular quadrature QND measurement of the pump mode via a signal phase measurement, which naturally provides a way to deterministically generate optical GKP logical states with additional all-Gaussian resources. Combined with the all-Gaussian GKP magic state distillation protocol from GKP logical states [15], our results may unlock promising opportunities for room-temperature ultrafast universal quantum computation with GKP states in CV architectures. It is worth mentioning that our GKP state generation protocol uses Gaussian quadrature measurements, which can be purified using recently demonstrated amplification techniques with high-gain linear OPAs before the inefficient general-dyne measurements, thereby offering a way to generate highly pure GKP states [67,80,81]. Finally, extending the discussions to OPO physics, we show that continuous homodyne monitoring of the outcoupled pump field leads to conditional localization of the signal mode on squeezed photon-number states, thereby highlighting a unique opportunity to synthesize and characterize the intracavity nonclassical states in real time.

Our scheme does not rely on materials with cubic nonlinearity, and thus provides a clear path for overcoming the long-standing challenge of nonlinear-optical PNR QND schemes based on cross-phase modulation, where the self-phase modulation that inevitably accompanies cross-phase modulation leads to phase noise that is detrimental to the probe field [20–23,82]. Our work establishes a concise description of the nonlinear-optical parametric interactions beyond the conventional semiclassical picture, thereby showing a practical path toward large-scale, ultrafast, and fault-tolerant universal photonic quantum information processors at room temperature.

ACKNOWLEDGMENTS

This work was supported by the National Science Foundation under Grants No. CCF-1918549 and No. PHY-2011363. R.N. and A.M. gratefully acknowledge support from National Science Foundation Grants No. 1846273 and No. 1918549, AFOSR Grant No. FA9550-201-0040, and the NASA Jet Propulsion Laboratory. The authors thank NTT Research for financial and technical support. R.Y. is supported by a Stanford Q-FARM Ph.D. Fellowship and the Masason Foundation.

APPENDIX A: DERIVATIONS FOR THE ROTATING FRAME HAMILTONIAN

We provide the derivation for the Hamiltonian (1). We start from the single-mode $\chi^{(2)}$ Hamiltonian in the laboratory frame

$$\hat{H} = g(\hat{a}^{\dagger 2}\hat{b} + \hat{a}^2\hat{b}^\dagger) + \omega_a\hat{a}^\dagger\hat{a} + \omega_b\hat{b}^\dagger\hat{b}. \tag{A1}$$

We move to a rotating frame given by a unitary

$$\hat{U} = \exp\left(i\frac{\omega_b t}{2}\hat{a}^\dagger\hat{a} + i\omega_b t\,\hat{b}^\dagger\hat{b}\right). \tag{A2}$$

This transforms the Hamiltonian as

$$\begin{aligned}\hat{H} \mapsto\ & \hat{U}\hat{H}\hat{U}^\dagger + i(\partial_t\hat{U})\hat{U}^\dagger \\ =\ & g(\hat{a}^{\dagger 2}\hat{b} + \hat{a}^2\hat{b}^\dagger) + \delta\hat{a}^\dagger\hat{a},\end{aligned} \tag{A3}$$

with the frequency detuning $\delta = \omega_a - \omega_b/2$.

APPENDIX B: KRAUS OPERATORS FOR PNR DETECTION

We derive the Kraus operators of the PNR QND measurement implemented with the Hamiltonian $\hat{H}_D$. For the pump p-homodyne outcome of p_b, the postmeasurement signal state becomes

$$\left|\varphi_a'(p_b)\right\rangle = \langle p_b|\, e^{-i\hat{H}_D t}\,|\varphi_a(0)\rangle\,|\varphi_b(0)\rangle \tag{B1}$$

up to normalization, where $|p_b\rangle$ is an engenstate of $\hat{p_b}$ with eigenvalue p_b. For the target signal state

$$|\varphi_a(0)\rangle = \sum_{N_a=0}^{\infty}\alpha_{N_a}\,|N_a\rangle\,, \tag{B2}$$

we have

$$\begin{aligned}\left|\varphi_a'(p_b)\right\rangle &= \langle p_b|\sum_{N_a=0}^{\infty}\alpha_{N_a}e^{-i\Delta N_a t}\hat{D}_b(\gamma_{N_a})\,|N_a\rangle\,|\varphi_b(0)\rangle \\ &= \sum_{N_a=0}^{\infty}\alpha_{N_a}C_{N_a}(p_b)\,|N_a\rangle\,,\end{aligned} \tag{B3}$$

with $\gamma_{N_a} = id\,(N_a + 1/2)$ and

$$C_{N_a}(p_b) = e^{-i\Delta N_a t}\,\langle p_b - d(N_a + 1/2)|\varphi_b(0)\rangle\,. \tag{B4}$$

Equation (B3) can be summarized as

$$\left|\varphi_a'(p_b)\right\rangle = \hat{M}(p_b)\,|\varphi_a(0)\rangle \tag{B5}$$

using Kraus operators

$$\hat{M}(p_b) = \sum_{N_a=0}^{\infty} C_{N_a}(p_b)\,|N_a\rangle\,\langle N_a|\,. \tag{B6}$$

Assuming a squeezed vacuum with width w along the p quadrature as the pump probe state $|\varphi_b(0)\rangle$, we can analytically write the complex probability amplitude

$$C_{N_a}(p_b) = \frac{e^{-i\Delta N_a t} e^{-\frac{1}{4w^2}\left(p_b - d\left(N_a+\frac{1}{2}\right)\right)^2}}{(2\pi)^{1/4} w^{1/2}}, \tag{B7}$$

which is a Gaussian function centered at $p_b = d(N_a + 1/2)$ with width w.

The POVM of the QND measurement protocol $\hat{F}(p_b)$ can be readily obtained from the Kraus operators as

$$\begin{aligned}\hat{F}(p_b) &= \hat{M}^\dagger(p_b)\hat{M}(p_b)\\ &= \sum_{N_a=0}^{\infty} |C_{N_a}(p_b)|^2\,|N_a\rangle\,\langle N_a|\,.\end{aligned} \tag{B8}$$

Notice that the POVM fulfills a normalization condition $\int dp_b\,\hat{F}(p_b) = \mathbb{1}_a$.

It is worth mentioning that the POVM (B8) is not completely selective with respect to N_a, because the POVM is composed of a mixture of multiple squeezed-Fock-state projectors. For quantitative characterizations of such mixedness of the POVM, we introduce relative weights of squeezed-Fock-state projectors

$$W_{N_a}(p_b) = \frac{|C_{N_a}(p_b)|^2}{\sum_{N_a'=0}^{\infty} |C_{N_a'}(p_b)|^2}. \tag{B9}$$

To understand the physical interpretation of $W_{N_a}(p_b)$, it is insightful to consider how the squeezed photon number distribution of a premeasurement state (B2), i.e.,

$$|\langle N_a|\varphi_a(0)\rangle|^2 = |\alpha_{N_a}|^2, \tag{B10}$$

changes conditioned on the homodyne outcome p_b. Using Eq. (B5), we can denote the squeezed photon number distribution of the postmeasurement state as

$$|\langle N_a|\varphi_a'(p_b)\rangle|^2 = \mathcal{N}|\alpha_{N_a}|^2 W_{N_a}(p_b), \tag{B11}$$

with normalization constant $\mathcal{N}$. Comparing Eqs. (B10) and (B11), we can interpret $\{W_{N_a}(p_b)\}$ as conditional weights that are multiplied to the squeezed photon number distribution of the input state $|\alpha_{N_a}|^2$. In particular, when $W_{N_a}(p_b) = 1$ holds for a certain N_a, the postmeasurement state becomes a pure squeezed photon-number state $|N_a\rangle$.

APPENDIX C: ALL-GAUSSIAN GENERATION OF GKP STATES

We introduce the generation scheme of GKP states by means of a modular quadrature measurement using the nonlinear quantum behavior of an OPA. Our basic approach adapts the protocols using ponderomotive interactions introduced in Ref. [14,49].

For the following discussions, we denote a coherent excitation of the signal Bogoliubov excitation as $|A\rangle$. Physically, $|A\rangle$ is a displaced squeezed state and is an eigenstate of $\hat{A}$ with eigenvalue A. As an initial system state, we consider

$$|\varphi(0)\rangle = |A_0\rangle \int dx_b\,\varphi_b(x_b)\,|x_b\rangle\,, \tag{C1}$$

with $A_0 > 0$, and $\varphi_b(x_b)$ represents the x-quadrature amplitude of the initial pump state. After propagation through a frequency-detuned OPA for time t, we measure the phase of the signal mode via a general-dyne measurement [68–70]. This projects the signal state on a measurement basis spanned by states $\{\left|e^{i\phi}(A_0+\epsilon)\right\rangle\}$, where a displaced squeezed state $\left|e^{i\phi}(A_0+\epsilon)\right\rangle$ is parameterized by the radius $A_0 + \epsilon \geq 0$ and the phase ϕ. The details for the construction of a general-dyne measurement are provided in Appendix F.

For a given measurement outcome of ϵ and ϕ, the postmeasurement pump state becomes

$$\begin{aligned}\left|\varphi_b'\right\rangle &= \left\langle e^{i\phi}(A_0+\epsilon)\right|\, e^{-i\hat{H}_D t}\,|A_0\rangle\,|\varphi_b(0)\rangle\\ &= \int dx_b\,\left\langle A_0+\epsilon\left|e^{i(2\tilde{g}tx_b-\Delta t-\phi)}A_0\right.\right\rangle \varphi_b(x_b)\,|x_b\rangle\end{aligned} \tag{C2}$$

up to normalization. As a result, we can write the Kraus operators representing the measurement protocol as

$$\hat{M}(\epsilon,\phi) = \sqrt{\frac{A_0+\epsilon}{\pi}} \int dx_b\,C_{x_b}(\epsilon,\phi)\,|x_b\rangle\,\langle x_b|\,, \tag{C3}$$

where

$$\begin{aligned}C_{x_b}(\epsilon,\phi) = \exp\Big\{&-\frac{1}{2}(A_0^2 + (A_0+\epsilon)^2\\ &-2A_0(A_0+\epsilon)e^{i(2\tilde{g}tx_b-\Delta t-\phi)}\Big\}\end{aligned} \tag{C4}$$

is a complex amplitude.

When we use a "meter" signal state with an amplitude much greater than the noise level of a vacuum, the outcome of the signal measurement is expected to be exponentially localized around $|\epsilon| \ll A_0$. Assuming that this condition is

met, we can approximate Eq. (C4) as

$$C_{x_b}(\epsilon,\phi) \approx \sum_{n=-\infty}^{\infty} \exp\left\{-2A_0^2(\tilde{g}t)^2(x_b - x_n - x_\phi)^2\right\} \times \exp\left\{2iA_0^2\tilde{g}t(x_b - x_n - x_\phi)\right\}, \quad \text{(C5)}$$

where $x_n = n\mu$ and $x_\phi = (\Delta t + \phi)/2\tilde{g}t \pmod{\mu}$, with $\mu = \pi/\tilde{g}t$. Notice that Eq. (C5) exhibits multiple Gaussian peaks with width $\kappa = 1/2\sqrt{\pi}A_0$ separated by an equal distance μ.

For the generation of a GKP state, we specifically consider a p-squeezed pump state

$$\varphi_b(x_b) = \frac{w^{1/2}}{(2\pi)^{1/4}} e^{-\frac{w^2x_b^2}{4}}, \quad \text{(C6)}$$

whose width along the p quadrature is $w/4$. Also, we set the interaction time to $\tilde{g}t = \sqrt{\pi/2}$ so that $\mu = \sqrt{2\pi}$. For these parameters, the postmeasurement pump state becomes

$$\begin{aligned}
|\varphi_b'\rangle &\approx \sum_{n=-\infty}^{\infty} \int dx_b\, e^{-\frac{w^2x_b^2}{4}} \exp\left\{-2A_0^2(\tilde{g}t)^2(x_b - x_n - x_\phi)^2\right\} \\
&\quad \exp\left\{2iA_0^2\tilde{g}t(x_b - x_n - x_\phi)\right\} |x_b\rangle \\
&\approx \sum_{n=-\infty}^{\infty} e^{-\frac{w^2(x_n+x_\phi)^2}{4}} \hat{D}_b(x_\phi)\hat{D}_b(x_n)\hat{D}_b(i\sqrt{\pi/2}A_0^2)\,|\kappa\rangle \\
&= \hat{D}_b(x_\phi)\hat{D}_b(i\sqrt{\pi/2}A_0^2) \sum_{n=-\infty}^{\infty} e^{-i\sqrt{2\pi}A_0^2x_n} \\
&\quad \times e^{-\frac{w^2(x_n+x_\phi)^2}{4}} \hat{D}_b(x_n)\,|\kappa\rangle\,, \quad \text{(C7)}
\end{aligned}$$

where we have ignored overall normalization constants. Here, $|\kappa\rangle$ is an x-squeezed vacuum with width κ along the x quadrature. Assuming that $|\kappa\rangle$ is strongly squeezed, we can perform an approximation

$$\begin{aligned}
&e^{-i\sqrt{2\pi}A_0^2x_n}\hat{D}_b(x_n)\,|\kappa\rangle \\
&= e^{-2\pi inA_0^2}\hat{D}_b(x_n)\,|\kappa\rangle \\
&= e^{-2\pi in(A_0^2 - \lfloor A_0^2\rfloor)}\hat{D}_b(x_n)\,|\kappa\rangle \\
&= e^{-i\sqrt{2\pi}(A_0^2 - \lfloor A_0^2\rfloor)x_n}\hat{D}_b(x_n)\,|\kappa\rangle \\
&\approx e^{-i\sqrt{2\pi}(A_0^2 - \lfloor A_0^2\rfloor)\hat{x}}\hat{D}_b(x_n)\,|\kappa\rangle \\
&= \hat{D}_b\left(-i\sqrt{\pi/2}(A_0^2 - \lfloor A_0^2\rfloor)\right)\hat{D}_b(x_n)\,|\kappa\rangle\,, \quad \text{(C8)}
\end{aligned}$$

where $\lfloor\cdot\rfloor$ is a floor function. This allows us to rewrite the postmeasurement state as

$$|\varphi_b'\rangle \approx \hat{D}_b(x_\phi)\hat{D}_b\left(i\sqrt{\pi/2}\lfloor A_0^2\rfloor\right)\left|\tilde{0}\right\rangle, \quad \text{(C9)}$$

where

$$\left|\tilde{0}\right\rangle \propto \sum_{n=-\infty}^{\infty} e^{-\frac{w^2(n\sqrt{2\pi}+x_\phi)^2}{4}} \hat{D}_b(n\sqrt{2\pi})\,|\kappa\rangle \quad \text{(C10)}$$

is an approximate GKP logical state. Notice that feedforward displacement operations based on the generaldyne measurement result can transform Eq. (C9) into an approximate GKP state.

APPENDIX D: EXPERIMENTAL REQUIREMENTS FOR THE PNR QND MEASUREMENT

We study the experimental requirements for the implementation of a PNR QND measurement scheme in the single-photon regime. In the presence of dissipation, the density matrix for the system state follows the master equation

$$\frac{d\hat{\rho}}{dt} = -i[\hat{H},\hat{\rho}] + \sum_{j\in\{a,b\}}\left(\hat{L}_j^\dagger\hat{\rho}\hat{L}_j - \frac{1}{2}\{\hat{\rho},\hat{L}_j^\dagger\hat{L}_j\}\right), \quad \text{(D1)}$$

where $\{\hat{O}_1,\hat{O}_2\} = \hat{O}_1\hat{O}_2 + \hat{O}_2\hat{O}_1$ is an anticommutator. In the main text, we assumed the dynamical timescale of the phase rotation of the Bogoliubov excitation Δ dominates over the nonlinear coupling rate, i.e., $\Delta \gg g$. Here we further assume that Δ dominates over the timescale of dissipation as well, i.e., $\Delta \gg \kappa_a, \kappa_b$. When this assumption holds, by virtue of the rotating-wave approximation, we are justified to ignore contributions from the rapidly rotating terms terms containing $\hat{A}^2$ and $\hat{A}^{\dagger 2}$ in Eq. (D1). Specifically, for the terms describing signal loss, we have

$$\hat{L}_a^\dagger\hat{\rho}\hat{L}_a - \frac{1}{2}\{\hat{\rho},\hat{L}_a^\dagger\hat{L}_a\} \approx \sum_{j\in\{+,-\}}\hat{L}_j^\dagger\hat{\rho}\hat{L}_j - \frac{1}{2}\{\hat{\rho},\hat{L}_j^\dagger\hat{L}_j\}, \quad \text{(D2)}$$

with $\hat{L}_+ = \sqrt{\kappa_a}\sinh(u)\hat{A}^\dagger$ and $\hat{L}_- = \sqrt{\kappa_a}\cosh(u)\hat{A}^\dagger$. This result indicates that, under a rotating-wave approximation, we can decompose the effect of the original signal Lindblad operator $\hat{L}_a = \sqrt{\kappa_a}\hat{a}$ into that of two Lindblad operators $\hat{L}_+$ and $\hat{L}_-$.

In the following discussions, for concreteness, we consider a squeezed single-photon state $|N_a = 1\rangle$ as an initial signal state. For the initial pump state, we assume a p-squeezed vacuum with width w along the p quadrature. For a successful PNR QND measurement, the probability for a quantum jump to occur in the signal mode should be sufficiently low. In the low-loss limit, the probability for a

quantum jump is approximately given as

$$\begin{aligned} P_{\text{jump}} &= 1 - \langle N_a = 1 | e^{-\hat{L}_a^\dagger \hat{L}_a t} | N_a = 1 \rangle \\ &\approx 1 - \langle N_a = 1 | e^{-(\hat{L}_+^\dagger \hat{L}_+ + \hat{L}_-^\dagger \hat{L}_-)t} | N_a = 1 \rangle \\ &= 1 - \langle N_a = 1 | e^{-\kappa_a (\cosh(2u)\hat{N}_a + \sinh^2(u))t} | N_a = 1 \rangle \\ &= 1 - e^{-\kappa_a (3\cosh^2(u) - 2)t}, \end{aligned} \tag{D3}$$

which sets a characteristic timescale for the loss-induced quantum jump as $t_{\text{jump}} \sim 1/\cosh^2(u)\kappa_a$.

To be able to measure $\hat{N}_a$ with high confidence, the conditional displacement occurring over the timescale of t_{jump} needs to be greater than the characteristic width of the pump state. In the presence of finite but small pump loss, the width of the final pump state along the p quadrature becomes

$$\begin{aligned} w'(t) &= \sqrt{w^2 e^{-\kappa_b t} + (1 - e^{-\kappa_b t})/4} \\ &\approx \sqrt{w^2 + (1/4 - w^2)\kappa_b t}, \end{aligned} \tag{D4}$$

where we have assumed $\kappa_b t \ll 1$. As a result, the experimental condition for a successful implementation of our scheme becomes $\tilde{g} t_{\text{jump}} \gtrsim w'(t_{\text{jump}})$. We use the squiggly symbol to denote approximate equality up to factors of order of unity.

We assume strong squeezing for all the fields involved, i.e., signal Bogoliubov excitation and the pump state. Also, we assume a similar level of loss and squeezing for both the signal and the pump, i.e., $\kappa_a \sim \kappa_b$ and $w \sim e^{-u} \ll 1$. Under these conditions, the order of magnitude of $w'(t_{\text{jump}})$ is larger than w by only a factor of unity, allowing us to approximate $w'(t_{\text{jump}}) \sim w$. As a result, we obtain a concise expression for the experimental requirement for our scheme as

$$\frac{g}{\kappa_a} \gtrsim w. \tag{D5}$$

APPENDIX E: LOSS ANALYSIS FOR EXTERNAL SQUEEZERS

In the main text, we comment on the possible extension of the PNR QND measurement scheme using external squeezing operations to modify the measurement basis. As illustrated in Fig. 5, we consider applying a pair of opposite squeezing operations $\hat{S}_a$ and $\hat{S}_a^\dagger$ to the signal state before and after the frequency-detuned OPA. In this construction, the frequency-detuned OPA implements a QND measurement of the squeezed photon number $\hat{N}_a$, and the external squeezing operations modify the overall measured observable to $\hat{N}_{\text{eff}} = \hat{S}_a^\dagger \hat{N}_a \hat{S}_a$, providing a flexible control to the measurement basis. A particular scenario of interest is when $\hat{S}_a$ is chosen such that $\hat{N}_{\text{eff}} = \hat{n}_a$ holds, which

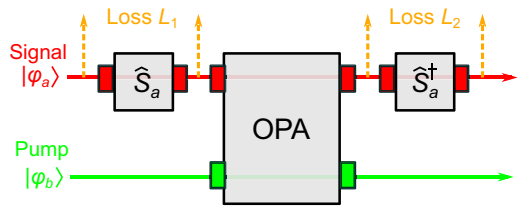

FIG. 5. The construction of an extended PNR QND measurement. The external squeezing operations modify the measured observable to $\hat{N}_{\text{eff}} = \hat{S}_a^\dagger \hat{N}_a \hat{S}_a$. We model the loss of each squeezer by a pair of equal beam splitters placed before and after the squeezer.

realizes a QND measurement of normal photon number as a whole. For an experimental implementation of such extended PNR QND measurements, the loss associated with the squeezers can induce measurement errors. In the following, we analyze the effects of squeezer-induced loss on the extended QND measurement for the case $\hat{N}_{\text{eff}} = \hat{n}_a$.

To separately analyze the effects of squeezer-induced loss from the effects of other possible imperfections, we assume ideal dynamics with no decoherence for the frequency-detuned OPA. We model a lossy squeezer with a total loss of L as a combination of an ideal squeezer and two beam splitters with equal transmissivity $T^2 = \sqrt{1-L}$ placed before and after the squeezer. We denote the losses of the first and second squeezers as L_1 and L_2, respectively (see Fig. 5). For concreteness, we consider an input single-photon Fock state $|1\rangle = \hat{a}^\dagger |0\rangle$.

In the absence of loss, the state after the first squeezer is a pure state $\hat{S}_a |1\rangle$, while nonzero loss makes the output of the first squeezer a mixed state described by a density matrix $\hat{\rho}_1$. Then, the error induced by the squeezer loss can be characterized by the infidelity

$$\mathcal{E}_1 = 1 - \langle 1 | \hat{S}_a^\dagger \hat{\rho}_1 \hat{S}_a | 1 \rangle, \tag{E1}$$

which can be interpreted as the probability of finding states other than the expected state $\hat{S}_a |1\rangle$ at the output of the first squeezer. In Fig. 6(a), we show $\mathcal{E}_1$ as a function of the loss L_1 for various squeezing levels of $\hat{S}_a$. We note that the power gain required for the external squeezers G to realize $\hat{N}_{\text{eff}} = \hat{n}_a$ is determined solely by the ratio $\tilde{g}/g = \sinh(2u)$ via $G = e^{2u}$.

To analyze the effects of the second squeezer's loss separately from the effects of the first squeezer's loss, we assume $L_1 = 0$ for the following discussions. Since we also assume an ideal frequency-detuned OPA Hamiltonian, which commutes with $\hat{N}_a$, the input to the second squeezer is $\hat{S}_a |1\rangle$. In the absence of loss, the output of the second squeezer should be a single-photon state $|1\rangle$, while nonzero loss leads to a mixed output state described by a density matrix $\hat{\rho}_2$. We can then quantify the error induced by the

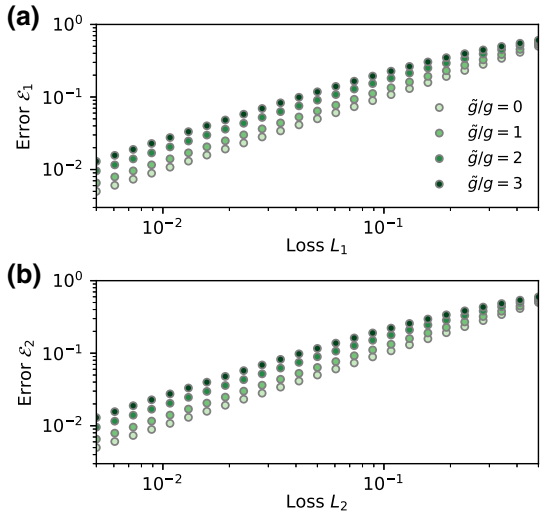

FIG. 6. Error induced by the loss of (a) the first squeezer and (b) the second squeezer for an extended PNR QND measurement with $\hat{N}_{\rm eff} = \hat{n}_a$. For $\tilde{g}/g = 1$, 2,and 3, respectively, the required power gain G of the external squeezer is 3.8, 6.3, and 7.9 dB.

loss of the second squeezer using the infidelity

$$\mathcal{E}_2 = 1 - \langle 1|\,\hat{\rho}_2\,|1\rangle\,, \tag{E2}$$

which we show as a function of L_2 in Fig. 6(b). Again, $\mathcal{E}_2$ can be interpreted as the probability of finding states other than the expected output state $|1\rangle$ at the end of the overall measurement protocol. We note that $\mathcal{E}_1$ and $\mathcal{E}_2$ exhibit similar but different values for the same level of squeezing and loss.

APPENDIX F: CONSTRUCTION OF GENERAL-DYNE MEASUREMENT

We introduce the construction of a general-dyne measurement [68]. The derivation follows Ref. [83]. Physically, a general-dyne measurement is a projection of a target state to a displaced squeezed state

$$\big|\phi_\xi(x+ip)\big\rangle = \hat{D}(x+ip)\hat{S}(\xi)\,|0\rangle\,, \tag{F1}$$

where $\hat{D}(\alpha)$ is a displacement operator and $\hat{S}(\xi)$ is a squeezing operator with a field gain ξ along the x quadrature. The POVM for the general-dyne measurement is given as

$$\hat{F}_\xi(x,p) = \frac{1}{\pi}|\phi_\xi(x+ip)\rangle\langle\phi_\xi(x+ip)|. \tag{F2}$$

Notice that the measurement basis becomes a coherent-state basis and an infinitely-squeezed-state basis for $\xi = 1$ and $\xi = \pm\infty$, respectively, and thus the notion of general-dyne measurement contains canonical heterodyne and homodyne measurements as special cases.

We illustrate our construction of a general-dyne measurement in Fig. 7, which we explain in detail below. First, we mix an input state $|\varphi\rangle_1$ in mode 1 with a vacuum state $|0\rangle_2$ in mode 2 with a beam splitter, and the state after the beam splitter becomes

$$|\varphi_{\rm BS}\rangle_{12} = \hat{U}_{\rm BS}\,|\varphi\rangle_1\,|0\rangle_2\,. \tag{F3}$$

We denote the unitary for a beam splitter with transmissivity $T = \cos^2\theta$ as

$$\hat{U}_{\rm BS} = \exp\Big\{\theta(\hat{a}_1\hat{a}_2^\dagger - \hat{a}_1^\dagger\hat{a}_2)\Big\}, \tag{F4}$$

where $\hat{a}_1$ and $\hat{a}_2$ are the annihilation operators for mode 1 and mode 2, respectively. The beam splitter unitary is characterized by the operator transformations [84]

$$\hat{U}_{\rm BS}^\dagger\hat{a}_1\hat{U}_{\rm BS} = \cos\theta\,\hat{a}_1 - \sin\theta\,\hat{a}_2, \tag{F5}$$

$$\hat{U}_{\rm BS}^\dagger\hat{a}_2\hat{U}_{\rm BS} = \sin\theta\,\hat{a}_1 + \cos\theta\,\hat{a}_2. \tag{F6}$$

We then perform x-quadrature and p-quadrature homodyne measurements on mode 1 and mode 2, respectively, yielding measurement outcomes $\hat{x}_1 = x_1$ and $\hat{p}_2 = p_2$. As a result, the post-beam-splitter state $|\varphi_{\rm BS}\rangle_{12}$ is projected onto the measurement basis $\{|x_1\rangle_1\,|p_2\rangle_2\}$, and this projection takes the form

$$\langle x_1|_1\,\langle p_2|_2\,|\varphi_{\rm BS}\rangle_{12} = \langle\phi(x_1,p_2)|\varphi\rangle_1\,. \tag{F7}$$

The whole process can be seen as a projection of the input state $|\varphi\rangle_1$ to the measurement basis spanned by the states

$$|\phi(x_1,p_2)\rangle_1 = \langle 0|_2\,\hat{U}_{\rm BS}^\dagger\,|x_1\rangle_1\,|p_2\rangle_2\,. \tag{F8}$$

Equation (F8) can be further evaluated as

$$\begin{aligned}
|\phi(x_1,p_2)\rangle_1 &= \langle 0|_2\,\hat{U}_{\rm BS}^\dagger\,|x_1\rangle_1\,\frac{1}{\sqrt{\pi}}\int dx_2\,e^{2ix_2p_2}\,|x_2\rangle_2 \\
&= \frac{1}{\sqrt{\pi}}\,\langle 0|_2\int dx_2\,e^{2ix_2p_2}\,|\cos\theta\,x_1 + \sin\theta\,x_2\rangle_1 \\
&\quad |-\sin\theta\,x_1 + \cos\theta\,x_2\rangle_2 \\
&= \frac{1}{\sqrt{\pi}}\,\csc\theta\int dx_2'\,e^{2i\csc\theta\,x_2'p_2}\,\big\langle 0\big|-\sin\theta\,x_1 + \cot\theta\,x_2'\big\rangle_2 \\
&\quad \times\,\big|\cos\theta\,x_1 + x_2'\big\rangle_1
\end{aligned}$$

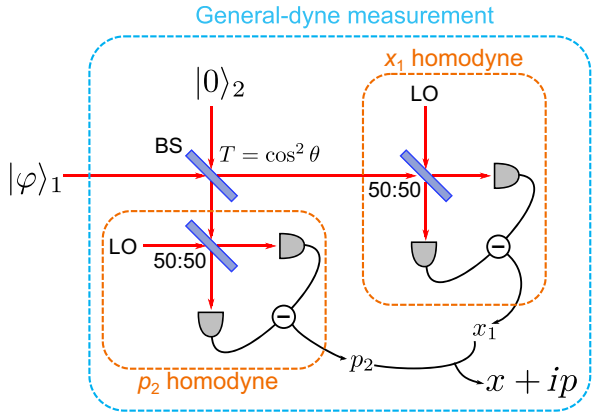

FIG. 7. Construction of a general-dyne measurement using two balanced homodyne detectors and one ancillary vacuum state. The overall measurement protocol projects the input state $|\varphi\rangle_1$ to a measurement basis spanned by displaced squeezed states $\{|\phi_\xi(x+ip)\rangle\}$. The outcome of the general-dyne measurement is related to the outcomes of the homodyne detectors via $x + ip = \sec\theta\, x_1 + i\csc\theta\, p_2$. The level of squeezing of the measurement basis $\xi = \tan\theta$ can be set via the choice of the beam splitter (BS) transmissivity $T = \cos^2\theta$. LO, local oscillator for a homodyne detector.

$$
\begin{aligned}
&= \frac{1}{\sqrt{\pi}} \csc\theta \int dx_1'\, e^{2i\csc\theta\,(x_1' - \cos\theta\, x_1)p_2}\, \langle 0| \\
&\quad \left|-\csc\theta\, x_1 + \cot\theta\, x_1'\right\rangle_2 \left|x_1'\right\rangle_1 \\
&= \frac{1}{\sqrt{\pi}} \csc\theta\, e^{-2i\cot\theta\, x_1 p_2} \int dx_1'\, e^{2i\csc\theta\, x_1' p_2} \times (2/\pi)^{1/4} \\
&\times e^{-\cot^2\theta (x_1' - \sec\theta\, x_1)^2} \left|x_1'\right\rangle_1 \\
&= \frac{e^{iv}}{\sqrt{\pi\, \sin\theta\cos\theta}} \hat{D}_1(\sec\theta\, x_1 + i\csc\theta\, p_2)\hat{S}_1(\tan\theta)\, |0\rangle_1 \\
&= \frac{e^{iv}}{\sqrt{\pi\, \sin\theta\cos\theta}} |\phi_\xi(x+ip)\rangle, \qquad \text{(F9)}
\end{aligned}
$$

where we have defined auxiliary variables $x_2' = \sin\theta\, x_2$ and $x_1' = x_2' + \cos\theta\, x_1$. In the final line, we have excluded the subscripts for the mode index for brevity. Here, e^{iv} is a known phase factor, $\xi = \tan\theta$, and

$$x = \sec\theta\, x_1, \quad p = \csc\theta\, p_2. \qquad \text{(F10)}$$

As a result, if we apply an appropriate normalization, the POVM for the entire measurement protocol becomes Eq. (F2), implying that we have successfully constructed a general-dyne measurement. The level of squeezing $\xi = \tan\theta$ can be set to any real value via the choice of the beam splitter transmissivity $T = \cos^2\theta$. For $\theta = 0, \pi/2$, the overall measurement becomes a homodyne measurement, while for $\theta = \pi/4$, the measurement becomes a heterodyne measurement.

To implement the phase measurement of $\hat{A}$ as discussed in Sec. III, we set the transmissivity of the beam splitter so that $\tan\theta = e^{-r}$ holds. Then, on the basis of the homodyne measurement outcomes x_1 and p_2, the state is projected to a desired measurement basis spanned by the displaced squeezed states $|A\rangle = |\phi_\xi(x+ip)\rangle$, with $A = x + ip$.

[1] M. A. Nielsen and I. L. Chuang, *Quantum Computation and Quantum Information* (Cambridge University Press, Cambridge, U.K., 2000).
[2] N. Gisin and R. Thew, Quantum communication, Nat. Photonics **1**, 165 (2007).
[3] The LIGO Collaboration, A gravitational wave observatory operating beyond the quantum shot-noise limit, Nat. Phys. **7**, 962 (2011).
[4] J. L. O'Brien, A. Furusawa, and J. Vučković, Photonic quantum technologies, Nat. Photon. **3**, 687 (2009).
[5] J. L. O'Brien, Optical quantum computing, Science **318**, 1567 (2007).
[6] M. A. Nielsen, Optical Quantum Computation Using Cluster States, Phys. Rev. Lett. **93**, 040503 (2004).
[7] S. L. Braunstein and P. van Loock, Quantum information with continuous variables, Rev. Mod. Phys. **77**, 513 (2005).
[8] N. C. Menicucci, P. van Loock, M. Gu, C. Weedbrook, T. C. Ralph, and M. A. Nielsen, Universal Quantum Computation with Continuous-Variable Cluster States, Phys. Rev. Lett. **97**, 110501 (2006).
[9] T. Rudolph, Why I am optimistic about the silicon-photonic route to quantum computing, APL Photonics **2**, 030901 (2017).
[10] S. Slussarenko and G. J. Pryde, Photonic quantum information processing: A concise review, Appl. Phys. Rev. **6**, 041303 (2019).
[11] Y. Li, P. C. Humphreys, G. J. Mendoza, and S. C. Benjamin, Resource Costs for Fault-Tolerant Linear Optical Quantum Computing, Phys. Rev. X **5**, 041007 (2015).
[12] S. Lloyd and S. L. Braunstein, Quantum Computation over Continuous Variables, Phys. Rev. Lett. **82**, 1784 (1999).
[13] S. Takeda and A. Furusawa, Toward large-scale fault-tolerant universal photonic quantum computing, APL Photonics **4**, 060902 (2019).
[14] D. Gottesman, A. Kitaev, and J. Preskill, Encoding a qubit in an oscillator, Phys. Rev. A **64**, 012310 (2001).
[15] B. Q. Baragiola, G. Pantaleoni, R. N. Alexander, A. Karanjai, and N. C. Menicucci, All-Gaussian Universality and Fault Tolerance with the Gottesman-Kitaev-Preskill Code, Phys. Rev. Lett. **123**, 200502 (2019).
[16] E. Knill, R. Laflamme, and G. J. Milburn, A scheme for efficient quantum computation with linear optics, Nature **409**, 46 (2001).
[17] R. H. Hadfield, Single-photon detectors for optical quantum information applications, Nat. Photon. **3**, 696 (2009).
[18] A. E. Lita, A. J. Miller, and S. W. Nam, Counting near-infrared single-photons with 95% efficiency, Opt. Express **16**, 3032 (2008).
[19] R. Nehra, A. Win, M. Eaton, R. Shahrokhshahi, N. Sridhar, T. Gerrits, A. Lita, S. W. Nam, and O. Pfister,

State-independent quantum state tomography by photon-number-resolving measurements, Optica **6**, 1356 (2019).
[20] N. Imoto, H. A. Haus, and Y. Yamamoto, Quantum nondemolition measurement of the photon number via the optical Kerr effect, Phys. Rev. A **32**, 2287 (1985).
[21] G. J. Milburn and D. F. Walls, Quantum nondemolition measurements via quadratic coupling, Phys. Rev. A **28**, 2065 (1983).
[22] B. He, Q. Lin, and C. Simon, Cross-Kerr nonlinearity between continuous-mode coherent states and single photons, Phys. Rev. A **83**, 053826 (2011).
[23] S. N. Balybin, A. B. Matsko, F. Y. Khalili, D. V. Strekalov, V. S. Ilchenko, A. A. Savchenkov, N. M. Lebedev, and I. A. Bilenko, Quantum nondemolition measurements of photon number in monolithic microcavities, Phys. Rev. A **106**, 013720 (2022).
[24] P. Grangier, J. A. Levenson, and J.-P. Poizat, Quantum non-demolition measurements in optics, Nature **396**, 537 (1998).
[25] J. F. Roch, G. Roger, P. Grangier, J.-M. Courty, and S. Reynaud, Quantum non-demolition measurements in optics: A review and some recent experimental results, Appl. Phys. B **55**, 291 (1992).
[26] K. Nemoto and W. J. Munro, Nearly Deterministic Linear Optical Controlled-NOT Gate, Phys. Rev. Lett. **93**, 250502 (2004).
[27] K. Nemoto and W. J. Munro, Universal quantum computation on the power of quantum non-demolition measurements, Phys. Lett. A **344**, 104 (2005).
[28] V. Venkataraman, K. Saha, and A. L. Gaeta, Phase modulation at the few-photon level for weak-nonlinearity-based quantum computing, Nat. Photon. **7**, 138 (2013).
[29] A. Negretti, U. V. Poulsen, and K. Mølmer, Quantum Superposition State Production by Continuous Observations and Feedback, Phys. Rev. Lett. **99**, 223601 (2007).
[30] J. M. Geremia, Deterministic and Nondestructively Verifiable Preparation of Photon Number States, Phys. Rev. Lett. **97**, 073601 (2006).
[31] M. Yanagisawa, Quantum Feedback Control for Deterministic Entangled Photon Generation, Phys. Rev. Lett. **97**, 190201 (2006).
[32] J. A. Levenson, I. Abram, T. Rivera, P. Fayolle, J. C. Garreau, and P. Grangier, Quantum Optical Cloning Amplifier, Phys. Rev. Lett. **70**, 267 (1993).
[33] A. Kuzmich and L. Mandel, Sub-shot-noise interferometric measurements with two-photon states, Quantum Semiclass. Opt. **10**, 493 (1998).
[34] V. Shah, G. Vasilakis, and M. V. Romalis, High Bandwidth Atomic Magnetometery with Continuous Quantum Nondemolition Measurements, Phys. Rev. Lett. **104**, 013601 (2010).
[35] G. Nogues, A. Rauschenbeutel, S. Osnaghi, M. Brune, J. M. Raimond, and S. Haroche, Seeing a single photon without destroying it, Nature **400**, 239 (1999).
[36] M. Brune, E. Hagley, J. Dreyer, X. Maître, A. Maali, C. Wunderlich, J. M. Raimond, and S. Haroche, Observing the Progressive Decoherence of the "Meter" in a Quantum Measurement, Phys. Rev. Lett. **77**, 4887 (1996).
[37] S. Gleyzes, S. Kuhr, C. Guerlin, J. Bernu, S. Deléglise, U. B. Hoff, M. Brune, J.-M. Raimond, and S. Haroche, Quantum jumps of light recording the birth and death of a photon in a cavity, Nature **446**, 297 (2007).
[38] R. J. Thompson, G. Rempe, and H. J. Kimble, Observation of Normal-Mode Splitting for an Atom in an Optical Cavity, Phys. Rev. Lett. **68**, 1132 (1992).
[39] H. J. Kimble, Strong interactions of single atoms and photons in cavity QED, Phys. Scr. **1998**, 127 (1998).
[40] D. Englund, A. Faraon, I. Fushman, N. Stoltz, P. Petroff, and J. Vučković, Controlling cavity reflectivity with a single quantum dot, Nature **450**, 857 (2007).
[41] A. Wallraff, D. I. Schuster, A. Blais, L. Frunzio, R.-S. Huang, J. Majer, S. Kumar, S. M. Girvin, and R. J. Schoelkopf, Strong coupling of a single photon to a superconducting qubit using circuit quantum electrodynamics, Nature **431**, 162 (2004).
[42] Y. Chu, P. Kharel, W. H. Renninger, L. D. Burkhart, L. Frunzio, P. T. Rakich, and R. J. Schoelkopf, Quantum acoustics with superconducting qubits, Science **358**, 199 (2017).
[43] K. Fukui, M. Endo, W. Asavanant, A. Sakaguchi, J. Yoshikawa, and A. Furusawa, Generating the Gottesman-Kitaev-Preskill qubit using a cross-Kerr interaction between squeezed light and Fock states in optics, Phys. Rev. A **105**, 022436 (2022).
[44] S. Pirandola, S. Mancini, D. Vitali, and P. Tombesi, Constructing finite-dimensional codes with optical continuous variables, EPL **68**, 323 (2004).
[45] R. W. Boyd, *Nonlinear Optics, 3rd edition* (Academic Press, New York, US, 2008).
[46] M. Zhao and K. Fang, InGaP quantum nanophotonic integrated circuits with 1.5% nonlinearity-to-loss ratio, Optica **9**, 258 (2022).
[47] J. Lu, M. Li, C.-L. Zou, A. Al Sayem, and H. X. Tang, Towards 1% single photon nonlinearity with periodically-poled lithium niobate microring resonators, Optica **7**, 1654 (2020).
[48] R. Yanagimoto, E. Ng, M. Jankowski, H. Mabuchi, and R. Hamerly, Temporal trapping: A route to strong coupling and deterministic optical quantum computation, Optica **9**, 1289 (2022).
[49] D. J. Weigand and B. M. Terhal, Realizing modular quadrature measurements via a tunable photon-pressure coupling in circuit QED, Phys. Rev. A **101**, 053840 (2020).
[50] P. Campagne-Ibarcq, A. Eickbusch, S. Touzard, E. Zalys-Geller, N. E. Frattini, V. V. Sivak, P. Reinhold, S. Puri, S. Shankar, R. J. Schoelkopf, L. Frunzio, M. Mirrahimi, and M. H. Devoret, Quantum error correction of a qubit encoded in grid states of an oscillator, Nature **584**, 368 (2020).
[51] H. W. Wiseman and G. J. Milburn, *Quantum Measurement and Control* (Cambridge University Press, Cambridge, UK, 2010).
[52] J. A. Medina-Vázquez, E. Y. González-Ramírez, and J. G. Murillo-Ramírez, Photonic crystal meso-cavity with double resonance for second-harmonic generation, J. Phys. B: At. Mol. Opt. Phys. **54**, 245401 (2022).

[53] J. Wang, M. Clementi, M. Minkov, A. Barone, J.-F. Carlin, N. Grandjean, D. Gerace, S. Fan, M. Galli, and R. Houdré, Doubly resonant second-harmonic generation of a vortex beam from a bound state in the continuum, Optica **7**, 1126 (2020).

[54] P. Krantz, M. Kjaergaard, F. Yan, T. P. Orlando, S. Gustavsson, and W. D. Oliver, A quantum engineer's guide to superconducting qubits, Appl. Phys. Rev. **6**, 021318 (2019).

[55] R. Yanagimoto, E. Ng, A. Yamamura, T. Onodera, L. G. Wright, M. Jankowski, M. M. Fejer, P. L. McMahon, and H. Mabuchi, Onset of non-Gaussian quantum physics in pulsed squeezing with mesoscopic fields, Optica **9**, 379 (2022).

[56] N. Quesada, L. G. Helt, M. Menotti, M. Liscidini, and J. E. Sipe, Beyond photon pairs—nonlinear quantum photonics in the high-gain regime: A tutorial, Adv. Opt. Photonics **14**, 291 (2022).

[57] P. Kinsler, M. Fernée, and P. D. Drummond, Limits to squeezing and phase information in the parametric amplifier, Phys. Rev. A **48**, 3310 (1993).

[58] W. Xing and T. C. Ralph, Pump depletion in parametric amplification, arXiv:2201.01372 [physics.optics] (2022).

[59] W. Qin, A. Miranowicz, and F. Nori, Beating the 3 dB Limit for Intracavity Squeezing and Its Application to Nondemolition Qubit Readout, Phys. Rev. Lett. **129**, 123602 (2022).

[60] W. J. Gu, Z. Yi, L. H. Sun, and D. H. Xu, Mechanical cooling in single-photon optomechanics with quadratic nonlinearity, Phys. Rev. A **92**, 023811 (2015).

[61] D. H. Santamore, A. C. Doherty, and M. C. Cross, Quantum nondemolition measurement of Fock states of mesoscopic mechanical oscillators, Phys. Rev. B **70**, 144301 (2004).

[62] R. Nehra, M. Eaton, C. González-Arciniegas, M. Kim, and O. Pfister, Loss tolerant quantum state tomography by number-resolving measurements without approximate displacements, arXiv:1911.00173 [quant-ph] (2019).

[63] J. M. Epstein, K. Birgitta Whaley, and J. Combes, Quantum limits on noise for a class of nonlinear amplifiers, Phys. Rev. A **103**, 052415 (2021).

[64] O. Castaños, R. López-Peña, M. A. Man'ko, and V. I. Man'ko, Squeeze tomography of quantum states, J. Phys. A: Math. Gen. **37**, 8529 (2004).

[65] A. Ibort, V. I. Man'ko, G. Marmo, A. Simoni, and F. Ventriglia, An introduction to the tomographic picture of quantum mechanics, Phys. Scr. **79**, 065013 (2009).

[66] R. Yanagimoto, T. Onodera, E. Ng, L. G. Wright, P. L. McMahon, and H. Mabuchi, Engineering a Kerr-Based Deterministic Cubic Phase Gate via Gaussian Operations, Phys. Rev. Lett. **124**, 240503 (2020).

[67] R. Nehra, R. Sekine, L. Ledezma, Q. Guo, R. M. Gray, A. Roy, and A. Marandi, Few-cycle vacuum squeezing in nanophotonics, Science **377**, 1333 (2022).

[68] A. Serafini, *Quantum Continuous Variables* (CRC Press, Boca Raton, US, 2017).

[69] H. M. Wiseman, Adaptive Phase Measurements of Optical Modes: Going Beyond the Marginal *Q* Distribution, Phys. Rev. Lett. **75**, 4587 (1995).

[70] M. A. Armen, J. K. Au, J. K. Stockton, A. C. Doherty, and H. Mabuchi, Adaptive Homodyne Measurement of Optical Phase, Phys. Rev. Lett. **89**, 133602 (2002).

[71] K. Fukui, A. Tomita, A. Okamoto, and K. Fujii, High-Threshold Fault-Tolerant Quantum Computation with Analog Quantum Error Correction, Phys. Rev. X **8**, 021054 (2018).

[72] J. E. Bourassa, R. N. Alexander, M. Vasmer, A. Patil, I. Tzitrin, T. Matsuura, D. Su, B. Q. Baragiola, S. Guha, G. Dauphinais, Krishna K. Sabapathy, Nicolas C. Menicucci, and Ish Dhand, Blueprint for a scalable photonic fault-tolerant quantum computer, Quantum **5**, 392 (2021).

[73] K. Takase, K. Fukui, A. Kawasaki, W. Asavanant, M. Endo, J. Yoshikawa, P. van Loock, and A. Furusawa, Gaussian breeding for encoding a qubit in propagating light, arXiv:2212.05436 [quant-ph] (2022).

[74] L. J. Mensen, B. Q. Baragiola, and N. C. Menicucci, Phase-space methods for representing, manipulating, and correcting Gottesman-Kitaev-Preskill qubits, Phys. Rev. A **104**, 022408 (2021).

[75] R. Y. Teh, F.-X. Sun, R. E. S. Polkinghorne, Q. Y. He, Q. Gong, P. D. Drummond, and M. D. Reid, Dynamics of transient cat states in degenerate parametric oscillation with and without nonlinear Kerr interactions, Phys. Rev. A **101**, 043807 (2020).

[76] T. Onodera, E. Ng, C. Gustin, N. Lörch, A. Yamamura, R. Hamerly, P. L. McMahon, A. Marandi, and H. Mabuchi, Nonlinear quantum behavior of ultrashort-pulse optical parametric oscillators, Phys. Rev. A **105**, 033508 (2022).

[77] H. Mabuchi and H. M. Wiseman, Retroactive Quantum Jumps in a Strongly Coupled Atom-Field System, Phys. Rev. Lett. **81**, 4620 (1998).

[78] J. Kerckhoff, M. A. Armen, D. S. Pavlichin, and H. Mabuchi, The dressed atom as binary phase modulator: Towards attojoule/edge optical phase-shift keying, Opt. Express **19**, 6478 (2011).

[79] G. Milburn and D. F. Walls, Production of squeezed states in a degenerate parametric amplifier, Opt. Commun. **39**, 401 (1981).

[80] Y. Shaked, Y. Michael, R. Z. Vered, L. Bello, M. Rosenbluh, and A. Pe'er, Lifting the bandwidth limit of optical homodyne measurement with broadband parametric amplification, Nat. Commun. **9**, 609 (2018).

[81] N. Takanashi, A. Inoue, T. Kashiwazaki, T. Kazama, K. Enbutsu, R. Kasahara, T. Umeki, and A. Furusawa, All-optical phase-sensitive detection for ultra-fast quantum computation, Opt. Express **28**, 34916 (2020).

[82] P. Kok, Effects of self-phase-modulation on weak nonlinear optical quantum gates, Phys. Rev. A **77**, 013808 (2008).

[83] U. Chabaud, T. Douce, D. Markham, P. van Loock, E. Kashefi, and G. Ferrini, Continuous-variable sampling from photon-added or photon-subtracted squeezed states, Phys. Rev. A **96**, 062307 (2017).

[84] S. Olivares, Quantum optics in the phase space: A tutorial on Gaussian states, Eur. Phys. J. Special Topics **203**, 3 (2012).